COUETTE FLOWS, ROLLERS, EMULSIONS, TALL TAYLOR CELLS, PHASE SEPARATION AND INVERSION, AND A CHAOTIC BUBBLE IN TAYLOR-COUTTE FLOW OF TWO IMMISCIBLE LIQUIDS

By

D. D. Joseph

P. Singh

and

K. Chen

IMA Preprint Series # 616

February 1990

COUETTE FLOWS, ROLLERS, EMULSIONS, TALL TAYLOR CELLS, PHASE SEPARATION AND INVERSION, AND A CHAOTIC BUBBLE IN TAYLOR-COUETTE FLOW OF TWO IMMISCIBLE LIQUIDS

D.D. Joseph, P. Singh, and K. Chen

Department of Aerospace Engineering and Mechanics, University of Minnesota

107 Akerman Hall, Minneapolis, MN 55455

ACKNOWLEDGEMENTS

This research was supported by the National Science Foundation, the Army Research Office, and the Department of Energy.

ABSTRACT

Oil and water in equal proportion are set into motion between horizontal concentric cylinders when the inner one rotates. Many different flows are realized and described. In one regime many large bubbles of oil are formed. In a range of speeds where the water is Taylor unstable and the oil Taylor stable, we get strange Taylor cells of emulsified fluids whose length may be three or even four times larger than normal. The length of cells appears to be associated with effective properties of a non-uniform emulsion, so the cell sizes vary along the cylinder. At much higher speeds we get a fine grained emulsion which behaves like a pure fluid with normal Taylor cells. A second focus of the paper is on the mathematical description of the apparently chaotic trajectory of a small oil bubble moving between an eddy pair in a single Taylor cells trapped between the oil bands of a banded Couette flow. We defined a discrete autocorrelation sequence on a binary sequence associated with left and right transitions in the cell to show that the motion of the bubble is chaotic. A formula for a macroscopic Lyapunov exponent for chaos on binary sequences is derived and applied to the experiment and to the Lorenz equation to show how binary sequences can be used to discuss chaos in continuous systems. We use our results and recent results of Feeny and Moon (1989) to argue that Lyapunov exponents for switching sequences are not convenient measures for distinguishing between chaos (short range predictability) and white noise (no predictability).

The flows which develop between our rotating cylinders depend strongly on the material properties of the two liquids. A third focus of the paper is on dynamically maintained emulsions of two immiscible liquids with nearly matched density. The two fluids are 20 cp silicone oil and soybean oil with a very small density difference and small interfacial tension. The two fluids are

two immiscible liquids with nearly matched density. The two fluids are 20 cp silicone oil and soybean oil with a very small density difference and small interfacial tension. The two fluids are vertically stratified by weight when the angular velocity is small. Then one fluid fingers into another. The fingers break into small bubbles driven by capillary instability. The bubbles may give rise to uniform emulsions which are unstable and break up into bands of pure liquid separated by bands of emulsified liquid. We suggest that the mechanics of band formation is associated with the pressure deficit in the wake behind each microbubble.

INTRODUCTION

Some of the phenomena which are now to be described extend results first given in the paper of Joseph, Nguyen, and Beavers (1984). This paper is the only one we know to report results of experiments on the flow of two immiscible liquids in a Taylor-Couette apparatus. We shall refer to this paper as JNB. The papers by Y. Renardy and D. Joseph (1985) and by Guillopé, Joseph, Nguyen, and Rosso (1987) are the only theoretical studies of the special form of two-fluid flow between rotating cylinders called Couette flow. The paper by Joseph and Preziosi (1987) gives a theoretical explanation of rollers, which is another configuration which appears in our experiments between cylinders. In this paper we are going to describe some of the flows which can be observed when two immiscible liquids are set into motion between horizontal cylinders when the inner one rotates. Many different flows are realized: fingering flows, coarse and fine emulsions, phase-separated emulsions, lubricated flow, and banded Couette flows.

The nature of fluid-solid interactions takes a more important place in two-fluid dynamics than in single fluid dynamics. There is a competition between the two fluids as to which one will wet a solid boundary. The factors that enter into this competition are not understood. We get some kind of interaction between the physical chemistry of adsorption of fluid at the boundary of a solid with two-fluid dynamics. Wetting is not determined entirely by energy considerations, by contact angles, static or dynamic. The history of the motion also plays an important role in determining the places on the solid which are wet by one liquid or another (see Figure 3e).

Taylor-Couette flows of a single fluid are among the best understood of all fluid phenomenon. One reason for this is that the geometry is relatively simple for analysis and perfectly marvelous for experiments. The Taylor-Couette apparatus may also evolve as an apparatus of choice in the study of two-fluid dynamics, fluid-solid interaction, and in the study of dynamical properties of emulsions.

EXPERIMENTS

All of the experiments were carried out between two concentric cylinders with axis horizontal, perpendicular to gravity. The outer cylinder and the end plates are plexiglass. The inside diameter of the outer cylinder is 2.495 inches; the outside diameter is 2.986 inches. The inner cylinder is of aluminum with a diameter of 1.985 inches. This is a convenient reference for normal Taylor cells which combine two counter-rotating eddies approximately 0.515 inches in length. The length of the cylinder is 11.985 inches. The outer cylinder is fixed and the inner one rotates with angular velocity Ω.

Our Taylor apparatus uses two neoprene lip seals to prevent leakage. The shaft driving the inner cylinder is connected to a torque meter which has a provision for counting rpm. The torque meter is connected to a mechanical-digital converter which displays the value of the torque and rate of rotation. The digital signal is transferred to a Hewlett-Packard 87 and then sample averaged. Usually there is a fluctuation in the torque before the rotation reaches a new steady state. By monitoring the values displayed on the digital converter, we can determine when the motion is in steady state. We took torque data for some of the experiments which is reported in Figure 1. For uniformity each data point was taken one-half hour after establishing a changed condition. Obvious transients were well delayed after this time. Sometimes there is a slow emulsification which will eventually change the dynamics.

The torque values shown in Figures 1, 5, and 9 are not guaranteed because there is an unknown frictional torque due to the neoprene seals which varies with the speed. The decrease in the torque at small values of Ω is almost certainly an effect of seals and not of flow. At higher speed the fraction of the total torque due to the bearings is smaller. Perhaps torques measured at speeds in excess of 80 rpm are reasonably accurate.

The laboratory is temperature controlled at 25° Celsius. We used two different oils in the experiments with water and oil: Mobil heavy duty oil with density of 0.97 g/cm^3 and viscosity 0.95 poise, and SAE 30 motor oil with density of 0.886 g/cm^3 and viscosity of 0.98 poise. The major effect of the density difference occur in slow or lubricated flow in which the oil floats up. This effect is greater in SAE 30 oil-water systems than in the heavy oil-water system which is more nearly density matched.

A different set of experiments in the same apparatus were carried out with silicone oil and soybean oil (under the brand name of Crisco). The density and viscosity of the silicone oil is $\rho = 0.949$ g/cm^3, $\mu = 0.2$ p and of the soybean oil is $\rho = 0.922$ g/cm^3, $\mu = 0.46$ p.

The interfacial tension between Mobil heavy-duty motor oil and tap water is 30.00 dyne/cm. The interfacial tension between SAE 30 motor oil and tap water is 9.2 dyne/cm. The interfacial tension between 0.2 p silicone oil and Crisco is 1.4 dyne/cm.

PARAMETERS

Six dimensionless parameters govern these flows: the viscosity ratio, the density ratio, the volume ratio, a capillary number, a Froude number based on $\Delta\rho g$ where $\Delta\rho$ is the density difference, and a Taylor (or Reynolds) number. We are going to collect data for systematic variations of the parameters later. It is useful to note that we usually get some form of emulsions when the Taylor number for the high viscosity constituent is larger than the critical one for Taylor instability. The critical angular velocities in our apparatus are calculated from the instability theory as [4.35, 409, 402, 91.7, 217] rpm for [water, SAE 30 motor oil, Mobil heavy-duty motor oil, 0.2 p silicone oil, Crisco] when one fluid rather than two fluids fills the gap. We say that two-phase flow between cylinders is bistable when one phase is stable, the other unstable. Bistable flow of water and motor oil occurs when $4.35 < \Omega < 409$ (or 402) rpm. Bistable flow of silicone and Crisco oil occurs when
$91.7 < \Omega < 217$ rpm.

COUETTE FLOWS

Couette flows of two liquids are here defined as steady axisymmetric flow of two immiscible liquids between infinitely long rotating cylinders of radius $a < b$ and angular velocities Ω_1 and Ω_2. These flows satisfy the Navier-Stokes equations, no-slip boundary conditions, and classical interface conditions at liquid-liquid interfaces. The Couette flows are a small class of steady and possibly nonaxisymmetric flows which could develop between rotating cylinders, but in contrast to the one-fluid case, Couette flows of two fluids are not unique, there a continuum of solutions of at least two different types: layered and banded Couette flows.

Layered Couette flows

Layered Couette flows are one class of steady solutions. For two layers, one is on the inside, two outside, and the interface between them is at $r = d$. In fact the steady solutions are not unique, there could be any number of layers of any thickness subject to the specification of the volume of each fluid and geometrical constraints. JNB showed that the layered flow with just two layers, the low viscosity liquid on the inner cylinder, uniquely minimizes the torque when the angular velocity difference is prescribed. They noted that the minimizing torque can be determined by minimization for two layers since we may always consider the problem for adjacent layers. For two layers, one inside, two outside, the torque M_L per length L is

$$M_L = \frac{a^2 b^2 (\Omega_2 - \Omega_1)}{(b^2 - a^2) k} \frac{\mu_1 \mu_2 (b^2 + k a^2) L}{(b^2 \mu_1 + k a^2 \mu_2)} \tag{1}$$

where

$$k = \frac{v_2}{v_1} \tag{2}$$

is the ratio of volumes. Suppose that we have oil and water, fixing the water volume v_W and oil volume. First we compute M when $\mu_1 = \mu_w$, $v_1 = v_w$; then compute M when $\mu_2 = \mu_w$, $v_2 = v_w$. The case with $\mu_1 = \mu_w$ gives a smaller torque, so the water is on the inner cylinder $r = a$, oil outside.

The stability of layered Couette flow was studied by Renardy and Joseph (1985) and Guillopé et al. (1988). The linear theory with gravity neglected studied in their paper showed that a thin layer of the less-viscous fluid next to either cylinder is linearly stable and that it is possible to have stability with the less dense fluid lying outside. The stable configuration with less-viscous fluid next to the outer cylinder, layered Couette flows, have never been observed because of effects neglected. However various lubricated flows with less viscous fluid on the wall in the presence of gravity could be regarded as realizations of the torque-minimizing layered Couette flow. For examples of this type we refer the reader to Figures 7, 8, and 9, and especially Figure 10 of JNB and to the description of the flows shown in Figures 2e, f, and g of this paper.

Banded Couette flows

These flows are such that the two fluids are arranged in alternating bands rather than layers. This is an exact solution, the same solution as if there were no bands.

$$\mathbf{u} = \mathbf{e}_\theta V(r) = \mathbf{e}_\theta\left(Ar + \frac{B}{r}\right),$$

$$A = \frac{b^2\Omega_2 - a^2\Omega_1}{b^2 - a^2}, \tag{3}$$

$$B = (\Omega_1 - \Omega_2)\frac{a^2b^2}{b^2 - a^2}.$$

The interface between bands are set on the annular areas in the intersection of the gap and planes perpendicular to axis z of the cylinders. The velocity is automatically continuous; the shear stresses $\tau_{z\theta}$ and τ_{zr} are zero and the pressure is continuous across these planes.

Banded Couette flows are not unique, the width of the bands and their number is not determined by stated conditions. The torque on the cylinders is the sum of the torques of each band. The torque M_B on a band of length L, with viscosity μ, is given by

$$M_B = \frac{L\mu}{2}\int_a^b r^3\left[\frac{d\left(\frac{v}{r}\right)}{dr}\right]^2 dr$$

$$= L\mu a^2 b^2 \frac{(\Omega_2 - \Omega_1)^2}{b^2 - a^2}. \tag{4}$$

Suppose L_1 is the total length of bands of fluid with viscosity μ_1 and L_2 with viscosity μ_2. Then

$$L_1 + L_2 = L,$$

$$\frac{L_2}{L_1} = \frac{V_2}{V_1} = k, \text{ and} \tag{5}$$

$$M_B = \frac{(\mu_2 + k\mu_1)}{1 + k} L a^2 b^2 \frac{(\Omega_2 - \Omega_1)^2}{b^2 - a^2}.$$

To compare the torques on the cylinders in banded and layered Couette flow we put

$$\frac{M_B}{M_L} = \frac{\left(b^2\mu_1 + ka^2\mu_2\right)}{\mu_1\mu_2\left(b^2 + ka^2\right)} \frac{(\mu_2 + k\mu_1)}{(1+k)}$$

$$= \frac{\left(m + k\frac{a^2}{b^2}\right)(1 + mk)}{m\left(1 + k\frac{a^2}{b^2}\right)(1+k)} \tag{6}$$

where

$$m = \frac{\mu_1}{\mu_2}.$$

The minimum torque in layered Couette flow is when the low viscosity constituent is on the wall, $m < 1$. The function (6) of m decreases from infinity at $m = 0$ to one at $m = 1$. Hence $M_B > M_L$; layered Couette flow has a smaller torque for the same angular velocity and volume fraction as banded Couette flow for which the oil must necessarily attach itself to both inner and outer layer.

Banded Couette flows are not lubricated. We have never seen a banded Couette flow without secondary motions, but the flows shown in Figures 3a and 10 are banded Couette flows in the water cells which have already become unstable to Taylor vortices. The active water cells in Figure 10 are the sites for the strange attractor which is described in the section, "Chaotic trajectories of oil bubbles in an unstable water cell."

ROLLERS

There can be a superficial resemblance between banded Couette flows and rollers. The rollers shown in Figures 26 and 28 of JNB look exactly like the banded Couette flows shown in Figure 10 of this paper, but the rollers are not attached to the outer cylinder; they rotate nearly as a rigid solid sheared only by water. Truncated rollers are shown in Figures 2e, f, and g.

EMULSIONS, TALL TAYLOR CELLS, CELL NUCLEATION

The generation of emulsion can occur in several ways. The fluids at rest are stratified by gravity. At slow speeds a stable interface of one fluid advances into the other. The advancing interface develops scallops at its leading edge as in Figure 2.1. These scallops become unstable and finger into the host fluid (Figures 4 and 6a). Bubbles form from capillary instability leading directly or eventually to emulsions. The average size of the bubbles in an emulsion decreases as the speed (shear) increases. A coarse emulsion has large oil bubbles (Figures 2c, d). All these emulsions are maintained by shearing. They collapse to stratification when the motion is stopped. Strictly speaking, emulsions are unsteady because the oil water interfaces are moving. We can realize transient uniform emulsions (Figures 4 and 6b), but they appear to be unstable because they *cannot* be maintained when the angular velocity of the inner cylinder is fixed (Figure 6c).

The forms taken by rotating flows of emulsions depend strongly on the fluids used. In the oil-water systems we get very long cells and the cell sizes are variable along the axis of the cylinder (Figures 2d, 3b, 3c). This nonuniformity may be due to a nonuniformity of the degree of emulsification, the bubble size, along the axis. In any event the long nonuniform cells are robustly stable to changes in the angular velocity. At much higher speeds the degree of emulsification increases and new cell boundaries nucleate, producing more cells. Eventually we get a very fine stable homogeneous emulsion which has square Taylor cells of the usual type (Figures 3d, 6e). These cells are robust; if the angular velocity is reduced the normal cells persist. This shows that fine emulsions have a different response than coarse emulsions even when the gap size and angular velocity are the same.

Typical sequences of flow types are exhibited in the photographs of heavy motor oil in water shown in Figure 2 and in the photographs of SAE 30 motor oil shown in Figure 3. Many of the transitions are evident also in the torque graph, Figure 1, associated with transitions in the heavy oil of Figure 2.

PHASE INVERSION

There is a critical $\phi = \frac{v_1}{v_1 + v_2} = \tilde{\phi}$ = for *phase inversion*, which we shall now define. In our experiments $0.6 < \tilde{\phi} < 0.7$; when $\phi < 0.6$, the liquid with the lower viscosity (silicone oil) fingers into the more viscous liquid (Crisco oil) and eventually we get silicone drops in Crisco oil. When $\phi \geq 0.7$, we can sketch the same Figure 4; but the words Crisco and silicone are interchanged because Crisco, rather than silicone oil, fingers. In either case, the bubbly emulsions which exist before phase separation are uniform without structure. The bubbly emulsions all have smaller torques than the pure low viscosity constant (silicone oil) when Ω is small (see Figure 4). The torque is an increasing function of volume fraction up to phase inversion; after inversion ($\phi >$ 0.7) the torque appears to decrease with increasing ϕ. The "effective viscosity" of bubbly emulsions is smaller than the viscosity of its lowest viscosity constituent in pure form (silicone oil). There is a preference for low viscosity fingers to penetrate into the high viscosity fluid, $\phi < 0.6$. Phase inversion shows that it is also possible to get a more viscous liquid to finger into a less viscous one.

The torque curves can be used to back out the effective viscosity of an emulsion. The effective viscosity of emulsified Crisco oil is smaller than the effective viscosity of emulsified Crisco oil after phase inversion.

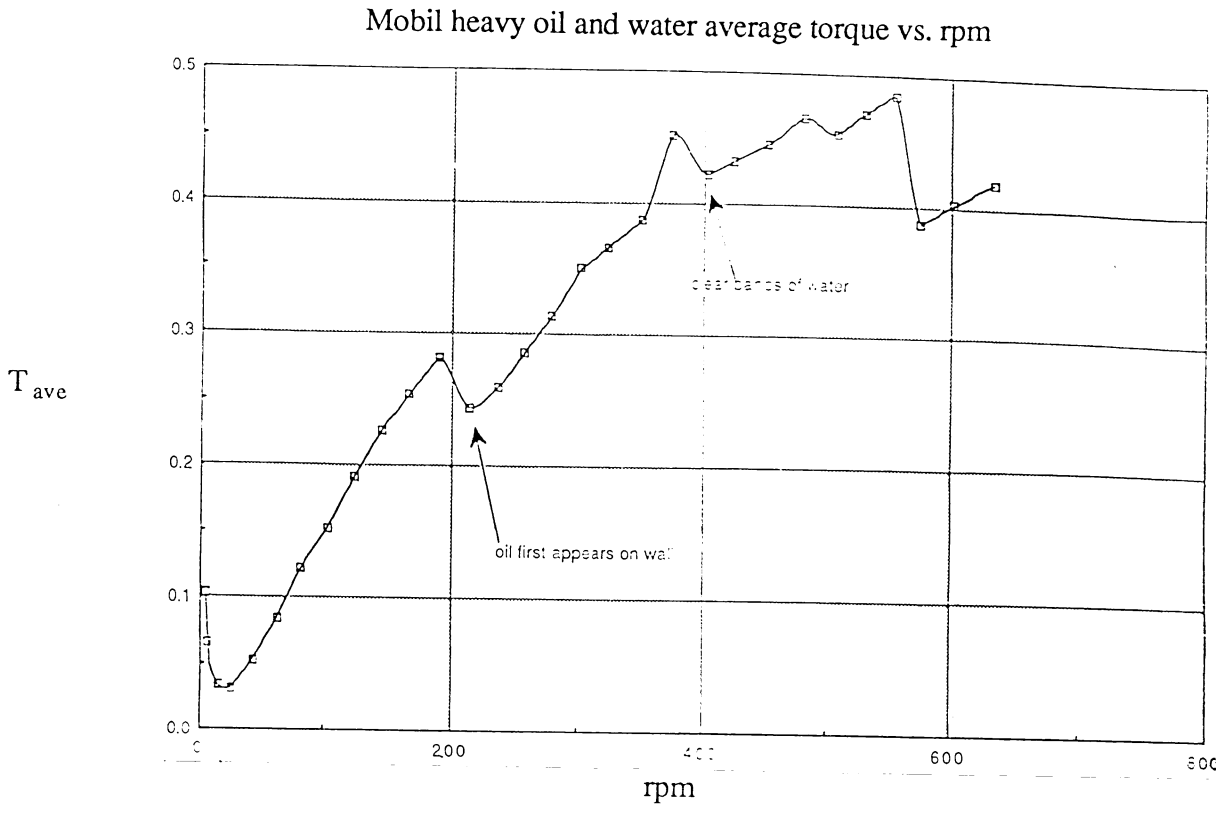

Fig. 1. Torque versus angular velocity for heavy motor oil and water. The decrease of the torque at the origin is due to the friction of the neoprene seal. We think that the oil foam which appears at $\Omega > 200$ marks the inflow boundary of a Taylor cell for a coarse grained emulsion. The appearance of clear bands is associated with spontaneous clearing of oil from the inner cylinder, increasing lubrication.

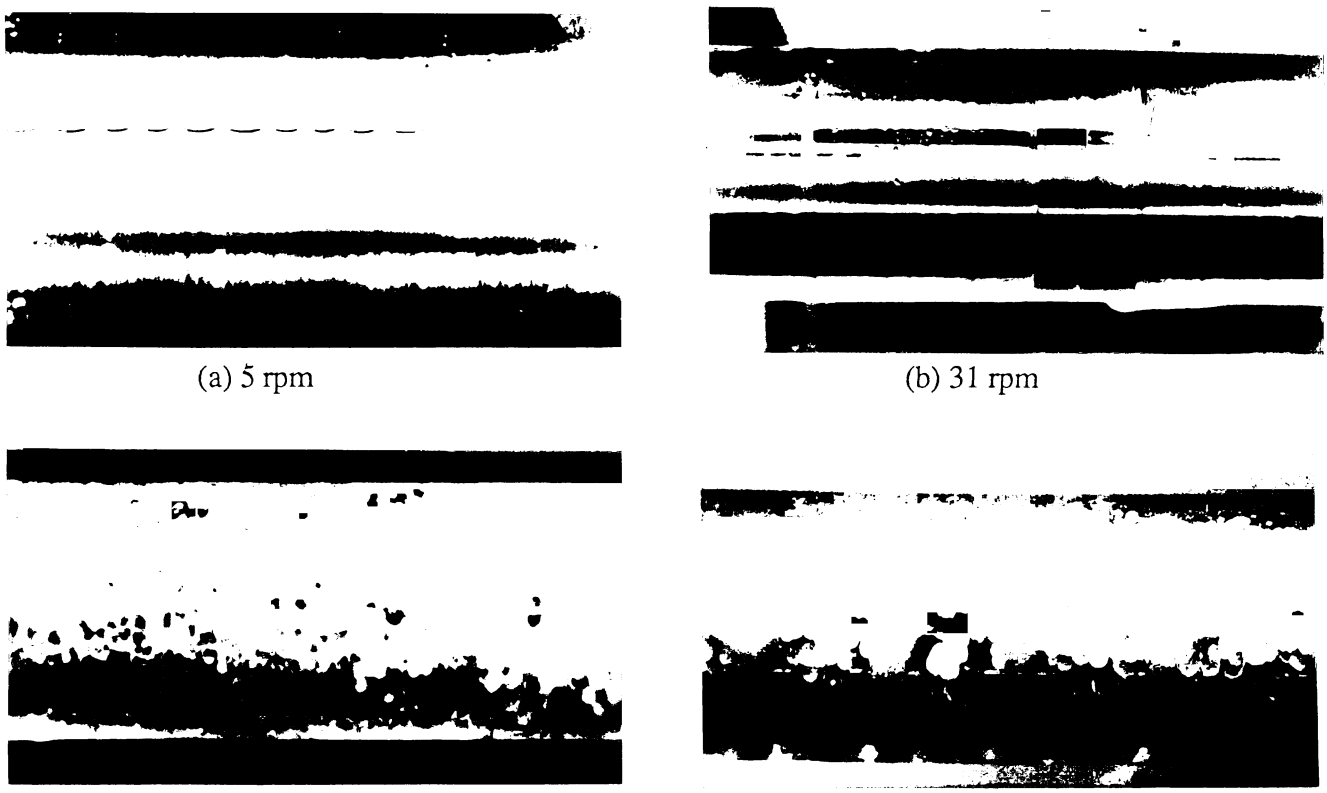

(a) 5 rpm (b) 31 rpm

(c) 201 rpm (d) 308 rpm

Fig. 2. Heavy motor oil and water. (a) 5 rpm. The inner cylinder is dragging the oil (top) into water (bottom). Scallops are on the leading edge of the oil-water interface which is steady and stable. (b) 31 rpm. The scalloped interface lost stability to a fat finger at 13 rpm. The finger was dragged around the cylinder and lead to the oil band evident in the photograph. There is a small oil roller on the left lubricated by water. (c) 201 rpm. This marks the beginning of a secondary motion of the oil bubbles. It appears that all of the oil has emulsified. A fine band of foamy oil is deposited on the outer cylinder over the inflow boundary. The cell size may be measured as a fraction of the outside diameter (0.29 inches). Normal Taylor cells are roughly twice the gap, 0.5 inches. These strange cells, which appear to be Taylor cells, are over three times as long as normal Taylor cells. We can treat the emulsion as an effective fluid with an effective viscosity. (d) 308 rpm. The oil bubbles are fine markers of the fluid motion elongating themselves in the direction of motion. The foamy oil bands are inflow boundaries. The outflow boundaries are between the inflow boundaries and define a center of orientational symmetry for the fluidized oil bubbles. The length of the cells is not uniform. The cells are three times longer than usual. *(Fig. 2 continued on next page.)*

(e) 500 rpm

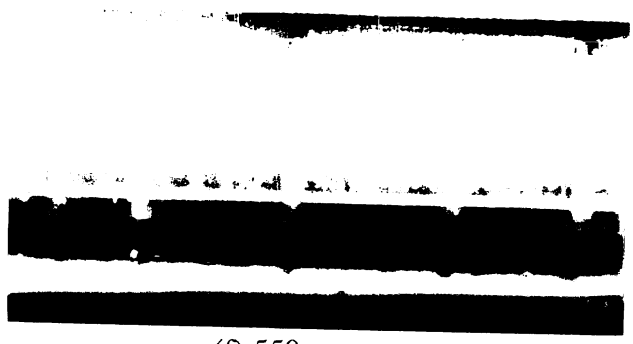

(f) 550 rpm

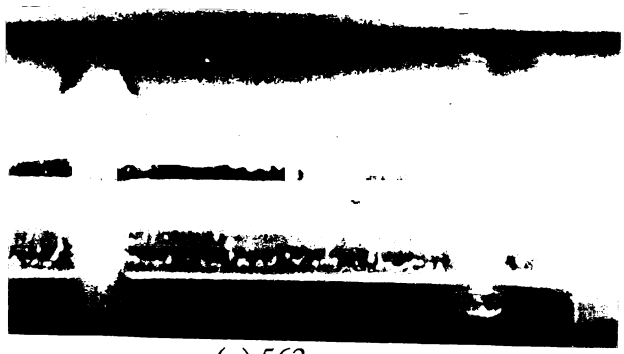

(g) 563 rpm

Fig. 2. *(continued)* Heavy motor oil and water. (e) 500 rpm. The emulsion has almost vanished. The oil on the outside cylinder is lubricated by water on the inside. Truncated rollers are on the inner cylinder. (f) 550 rpm. The oil at the top is shielded from the inner cylinder by a layer of water. It is a lubricated flow, like a layered Couette flow. There are well-lubricated oil rollers on the inner cylinder. (g) 563 rpm. There are bigger rollers and fewer drops. Everything is lubricated by water.

(a) 99 rpm

(b) 360 rpm

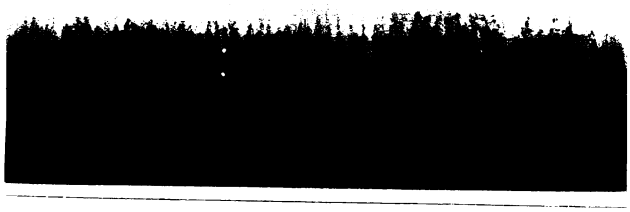

(c) 785 rpm

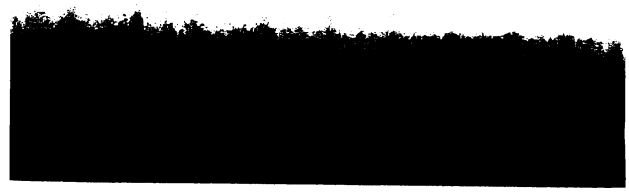

(d) 360 rpm

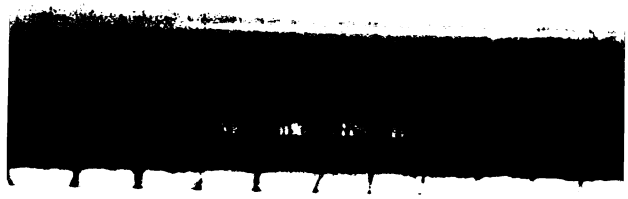

(e) 0 rpm

Fig. 3. SAE 30 motor oil and water, series 1. This series undergoes development somewhat like the one in Figure 2. (a) 99 rpm. A banded Couette is on the right and a water lubricated stratified flow on the left. The oil broke up at about 300 rpm and coarse grained emulsion is formed. (b) 360 rpm, (c) 785 rpm. The secondary motions are beautifully marked by the emulsions. The cell sizes are not uniform but do not change with speed. At higher speeds new cells nucleate and after several adjustments the long cells shorten to the normal length, twice the gap. This adjustment is complete at 2550 rpm. Then the speed is reduced to 360 rpm (d) and the normal cells are retained. The difference between (b) and (d) is due possible to the fact that the emulsion in (d) is finer. (e) The speed was reduced from 360 rpm to zero. The oil foam at the outside of the inflow boundary is stuck to the wall and it won't come off. This shows clearly that the fluid which wets the wall in different places depends on the history of the motion.

PHASE SEPARATION

Apparently the state of uniform emulsification is unstable. At least, we have never been able to maintain a state of uniform emulsification, even after one is created (see Figure 6). The instability of uniform emulsions in the silicone oil and Crisco oil systems leads to a phase separation. The cause of this phase separation is not understood. It could not be a form of Taylor instability since it occurs at angular velocities well below the critical Taylor number, 91.7, for the silicone oil alone. In fact the phase separation may occur at all finite values of the speed or rotation of the inner cylinder. We think that the state of uniform emulsification is unstable because of wakes which tend to align bubbles in rows. This effect is very clear in beds of spherical particles fluidized by water discussed in the paper by Fortes et al. (1987). In that case there is a scenario called drafting, kissing, and tumbling. Drafting is the mechanism by which one sphere is sucked into the wake of another, as debris is pulled from the side of a road behind a fast-moving truck. The rear

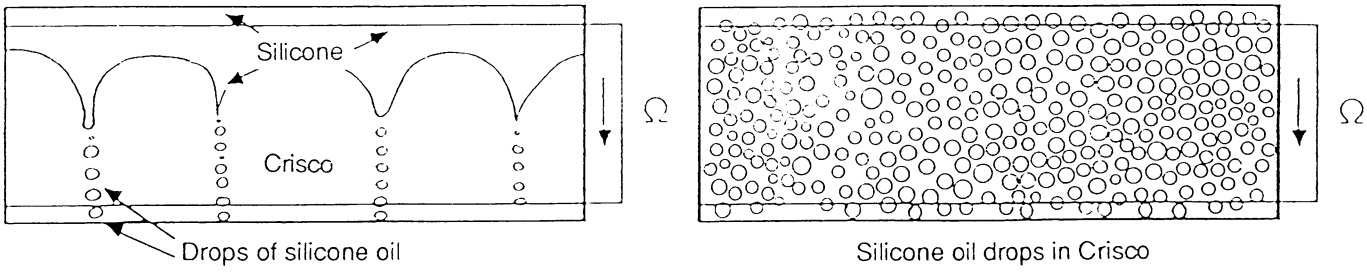

Fig. 4. Fingering instability leading to emulsion. The inner cylinder rotates.

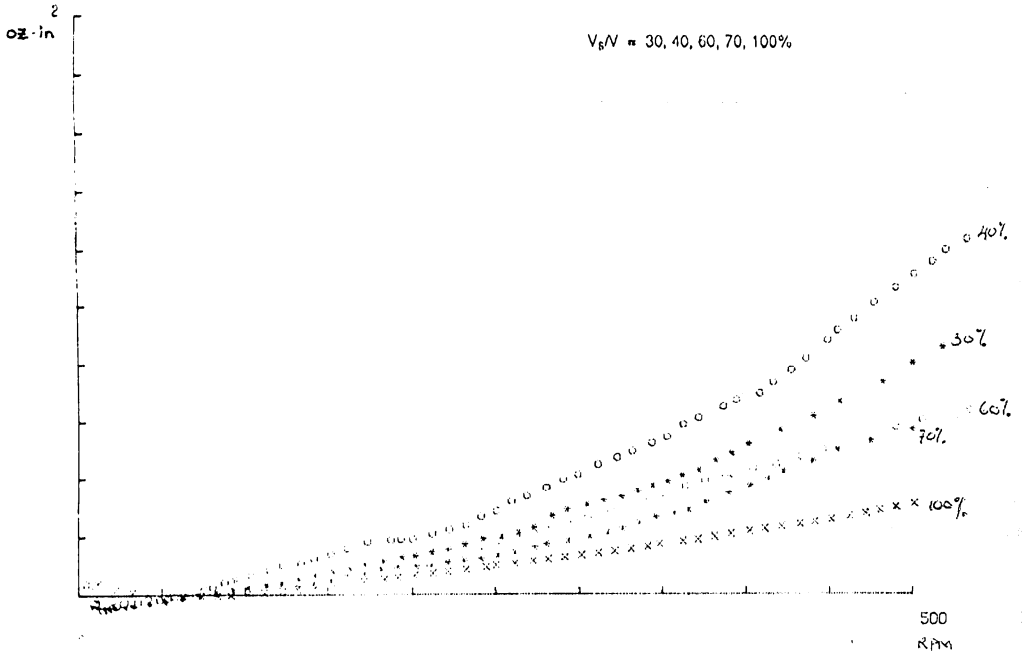

Fig. 5. Torque versus angular velocity with the volume fraction of silicone oil as a parameter.

sphere accelerates in the wake of the forward sphere and they kiss. The kissing spheres are aligned with stream. The kissing spheres form a long body which is unstable to the same kind of turning couples that cause and aircraft to stall so that spheres tumble into more stable cross stream pairs. Falling drops and rising bubbles also draft but they don't tumble. Instead, they appear to align as we have seen in drop experiments in which heavy liquids are dropped into a long tube filled with an immiscible lighter liquid.

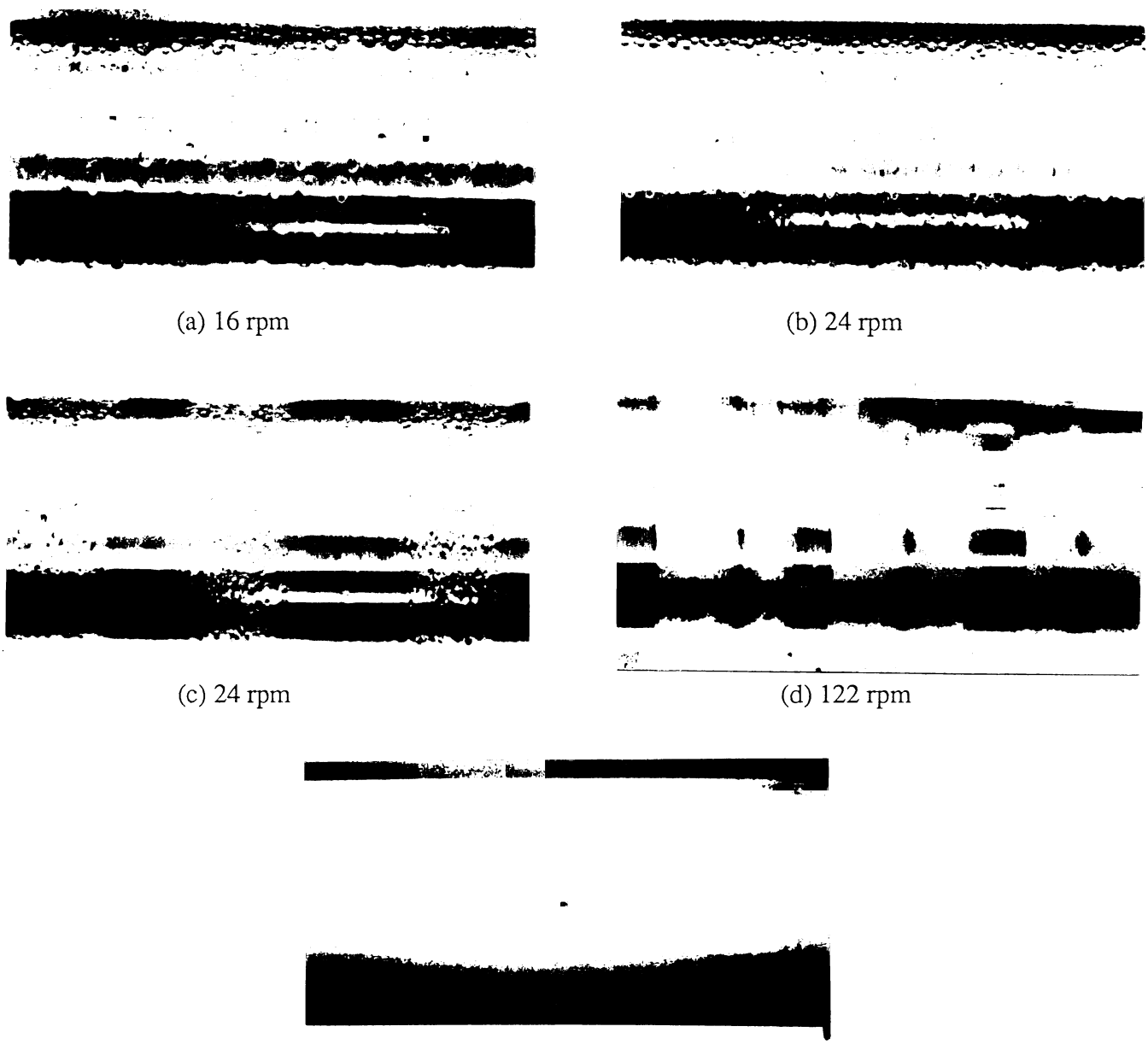

(a) 16 rpm

(b) 24 rpm

(c) 24 rpm

(d) 122 rpm

(e) 410 rpm

Fig. 6. Soybean (Crisco) oil and silicone oil in equal proportions. (a) 16 rpm. Silicone drops form as capillary instability after fingering. (b) "Uniform" emulsion at 24 rpm. (c) Phase separation at 24 rpm. (d) A finer emulsion of silicone oil at 122 rpm. Some of the phase boundaries are very distinct. (e) Stable emulsion with normal Taylor cells at 410 rpm.

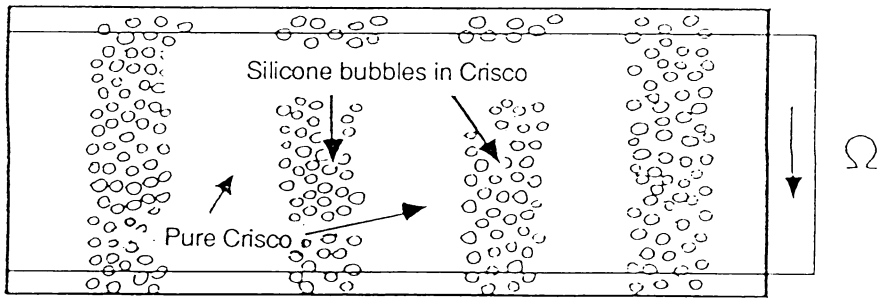

Fig. 7. Phase separation. Bands of emulsified silicone oil are separated by bands of pure Crisco oil, $\phi \leq 0.6$.

The drops always align and drafting is obvious. Side bubbles cannot be pulled uniformly in alignment, so there is a tendency to segregate. Clearly this explanation is tentative and incomplete.

PHASE INVERSION AND PHASE SEPARATION

When $\phi \leq 0.6$, symmetric equally spaced bands of an emulsion of silicone oil in Crisco are separated by bands of pure Crisco oil, as in Figure 7.

For $\phi = 0.7$, instead of silicone bubbles, we get Crisco bubbles, again with more or less symmetric equally spaced bands. In this case, a narrow band of pure Crisco oil is in the center of each band of emulsified Crisco oil, as in Figure 8.

The next event, as Ω increases, is the disappearance of the phase boundaries with uniform mixing, leading to a foamy emulsion that is unlike the grainy emulsion which develops after fingering. The foamy emulsions are more stable and take longer (5 to 10 minutes) to collapse when the rotation stops.

The appearance of foamy emulsions appears to coincide with the appearance of regular Taylor vortices. The secondary motion, which is generated from the instability of the hitherto stable Crisco oil in the bistable phase separated regime, may be the cause of the mixing leading to foamy emulsions. The critical angular velocity for the onset of Taylor vortices in the composite fluid, which we have called a foamy emulsion, can be determined visually; and, when the volume ration is small, $(\phi < 0.5)$ forms a sharp break in the torque curve (see Figure 9).

If we assume that this emulsion acts basically like a Newtonian fluid when in the Taylor apparatus, we can use the formula for the critical Taylor number to back out the value of the effective viscosity from the critical angular velocity, which is evidenced either by visual observation or by the break point in the angular velocity-torque curve.

The next critical Taylor number signals the formation of uniform wavy vortices in the foamy emulsion. We could also try to identify material properties from this transition.

Finally we note that at yet higher rotation rates the waves on the vortices seem to disappear, and, as far as the eye can see, the vortices are steady. This is unusual because it does not happen in the dynamics of Taylor vortices in single constituent liquids.

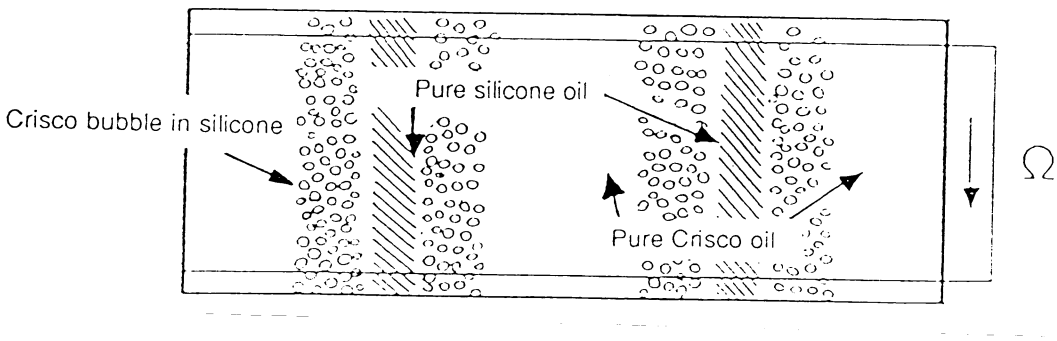

Fig. 8. Phase separation when Crisco oil fingers, $\phi = 0.7$.

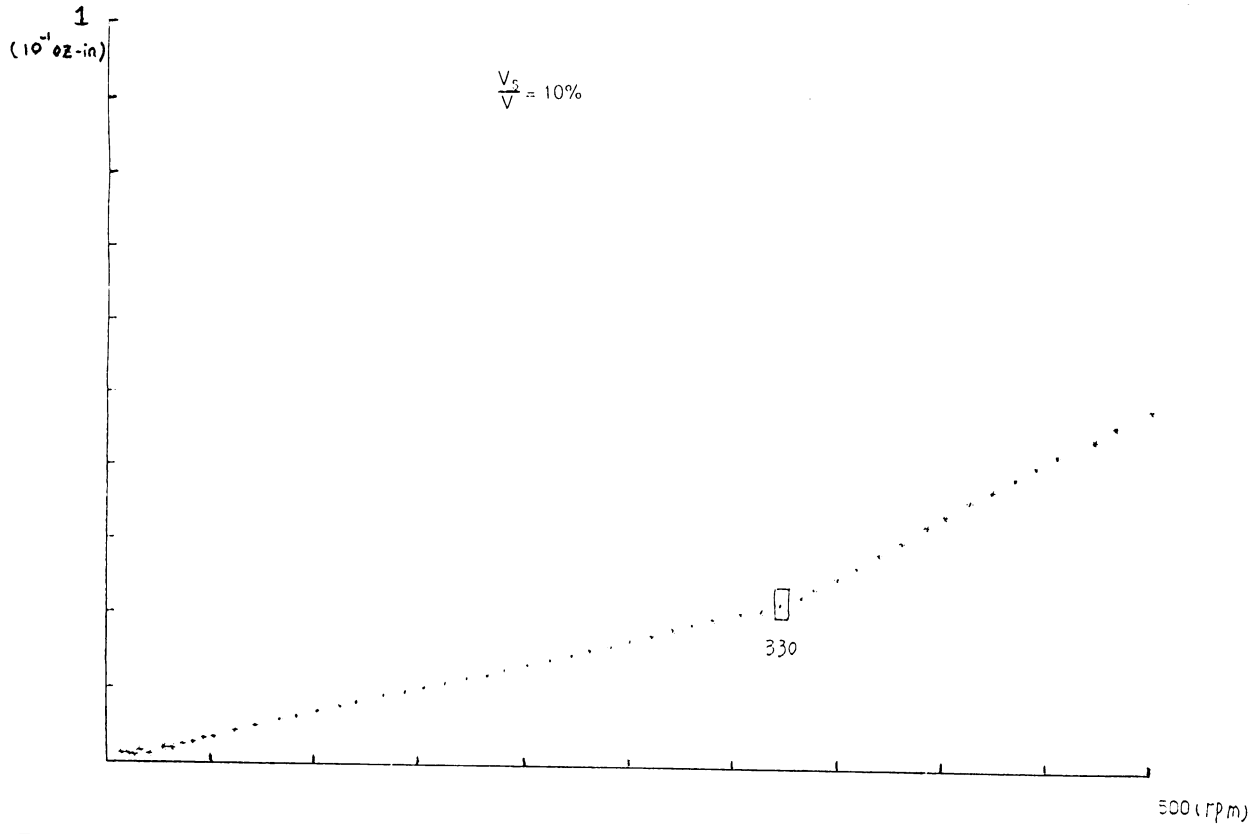

Fig. 9. Torque versus angular velocity for an emulsion of 10% silicone oil in Crisco. Taylor cells appear at 330 rpm.

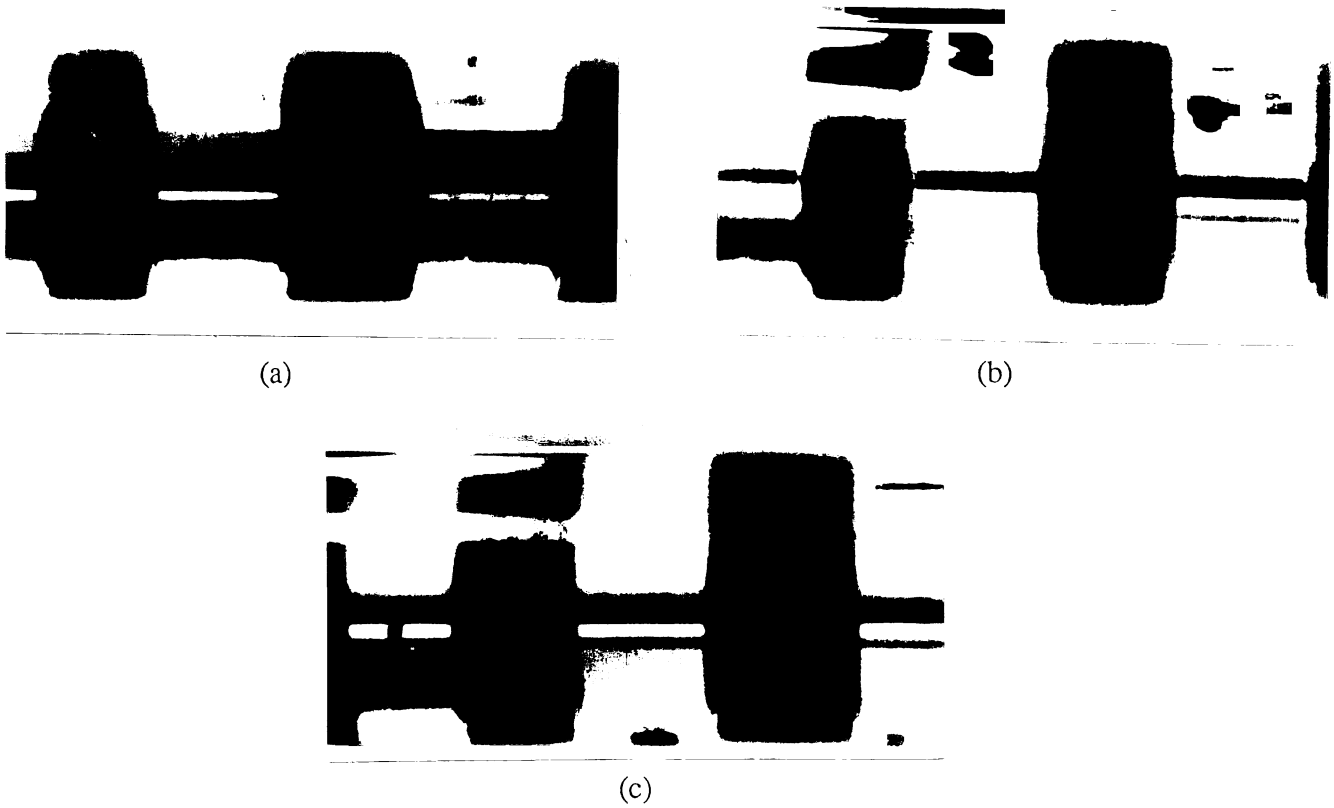

Fig. 10. Banded Couette flows of SAE 30 motor oil and water at 309 rpm. There is a small bubble in the unstable water cell on the left which is visible in (c) but not in (a) or (b). This small bubble undergoes an apparently chaotic motion. The large bubble appears to undergo chaotic switching from right to left.

CHAOTIC TRAJECTORIES OF OIL BUBBLES IN AN UNSTABLE WATER CELL

In the course of experiments described in the section, "Emulsions, tall Taylor cells, cell nucleation," we found a motion which appears to us to be chaotic. At sufficiently high values of the angular velocity prior to emulsification of motor oil, some bubbles of oil are torn away from the oil bands. In some situations we were able to get one oil bubble into a Taylor cell. This oil bubble is carried round and round by water and is dragged around in the secondary motion due to Taylor instability. We made a video tape of this and some still photographs are shown in Figure 10. The small oil bubble on the left is the one for which the binary sequence is studied. Each time the oil drop goes around it is either in the left eddy or in the right eddy. We monitored about 3000 terms in the sequence LRLL... and assigned number minus one to left and one to right. It is difficult to get revealing still photographs of the motion of the small bubble in the leftmost water cell shown in Figure 10. However, the large bubble in the center water cell also executes a chaotic motion of a slightly different type as can be seen in the photographs.

Binary sequences

We are going to apply methods of estimation theory (see Singh and Joseph, 1989) to characterize the chaos in the binary number sequence generated by the bubble in our experiments. Consider a sequence $u(n) = \pm 1$ of binary numbers. We assume that the sequence is ergodic so that time averages are the same as ensemble averages. In our experiment the average

$$E[u(n)] = \frac{1}{N}\sum_{n=1}^{N} u(n) \to 0$$

when N is large, left and right or ± 1 are equally probable.

Singh and Joseph (1989) showed how to generate a binary sequence for chaotic trajectories of the Lorenz system $[\dot{x}, \dot{y}, \dot{z}] = [\sigma(y - x), rx - y - xz, xy - bz]$ for $(\sigma, b, r) = (10, \frac{8}{3}, 28)$. The binary sequence is generated by projecting the trajectories into the xz plane, as shown in Figure 11, and monitoring the crossing points of trajectories on the segments AB and CD of the line AD. The crossing times are put into correspondence with the sequence n of integers, left crossings on AB are recorded as $u(n) = 1$, and the right crossings of CD, as $u(n) = -1$. The time averages of these sequences vanish for large N, independent of initial condition, so that left and right crossings are equally probably and we may assume that the sequences are ergodic.

Autocorrelations

An estimate of the autocorrelation function on an ergodic binary sequence can be obtained as follows:

$$r(n) = \frac{1}{N}\sum_{k=1}^{N} u(k+n)u(k), \quad n = 1, 2, \ldots \quad N \gg n. \tag{7}$$

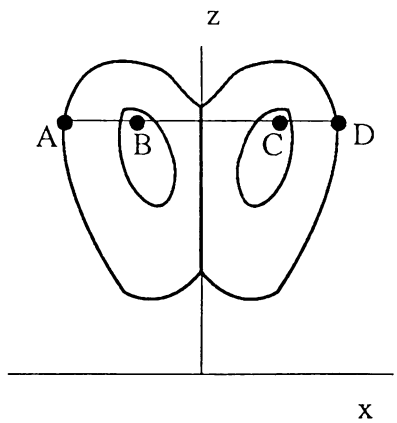

Fig. 11. The projected trajectories of the Lorenz attractor remain inside the butterfly region and outside the ovals around the fixed points.

The value r(1) represents the correlation between immediate neighbors (1, 2), (2, 3), (3, 4), etc. Value r(2) gives the correlation between separated pairs (1, 3), (2, 4), etc. A chaotic response is one for which $r(1) \neq 0$ and $r(n) \to 0$ for large n.

For the oil bubble autocorrelation values r(n)'s, for large n, are not uniformly close to zero because of the relatively small length of the sequence, $N = 3000$ (Figure 12). We tried sequences of different length and found that r(n)'s, for large n's, approached zero uniformly as the length of the sequence was increased.

The Lorenz equations were integrated numerically using the NAG library. Subroutine DO2BBF was used for different tolerance levels in the range 10^{-4} to 10^{-10}. We projected into the xz plane and formed a binary number symbol sequence with 76,000 entries. The autocorrelation function is shown in Figure 13. The tolerance level in the numerical scheme had absolutely no effect on the nature of autocorrelation sequence, even though sequences generated were quite different for different tolerance levels. For large n, r(n) approached zero uniformly with the increase in length of the sequence, N.

In both cases the decay in the autocorrelations value is very rapid. For large n, autocorrelation values decrease monotonically with the length of the sequence. The decay of autocorrelation for the bubble is essentially complete after $n = 2$, a substantial correlation exists only for r(1). The decay of correlation is slower for the Lorenz system with nonzero r(n) for $n < 6$. We could say that the Lorenz system is less random.

Lyapunov exponents

Singh and Joseph (1989) derived a macroscopic Lyapunov exponent for binary sequence. Lyapunov exponents for continuous times are locally defined quantities which measure the tendency for chaotic trajectories to diverge exponentially for small time, on the average. One can define the first exponent by

$$\lambda = \frac{1}{t_{N+1} - t_1} \sum_{k=1}^{N} \log_2 \frac{d(t_{k+1})}{d_0(t_k)} \tag{8}$$

where $d_0(t_k)$ is the initial distance between two trajectories at time t_k and $d(t_{k+1})$ is the distance between these two trajectories at time $t_{k+1} > t_k$. In the continuous case $d_0(t_k)$ and $d(t_{k+1})$ are infinitesimal and $N \to \infty$.

The concept of distance is not natural to binary sequences. Two trajectories correspond to two strings of binary symbols. We replace the condition that the initial distances between trajectories is small with the condition that we shall only compare strings of symbols which start with the same symbol. We can compare the "distance" between two strings of symbols which both start with u = 1 or both with –1, but not with starting values of +1 for one string and –1 for the other.

Another condition we need for comparing two strings of symbols is statistical independence. We want uncorrelated sequences so that theorems requiring ergocity, the use of "time" averages, will be appropriate. This requirement is easy to fulfill for our binary sequence symbol string. We compare two strings u(k), $k=1,2,\ldots$ with u(k+M) where M is larger than

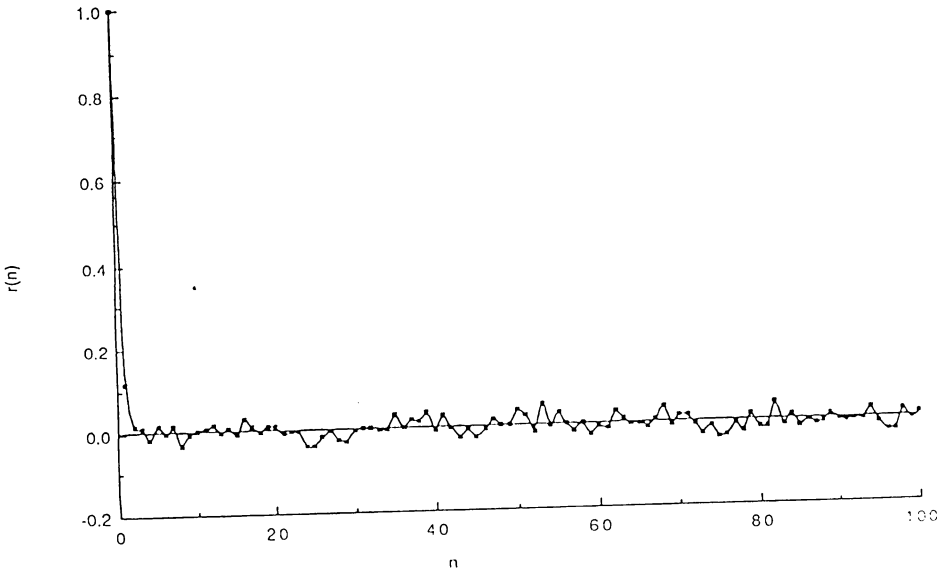

Fig. 12. The autocorrelation sequence for the oil bubble, N = 3000.

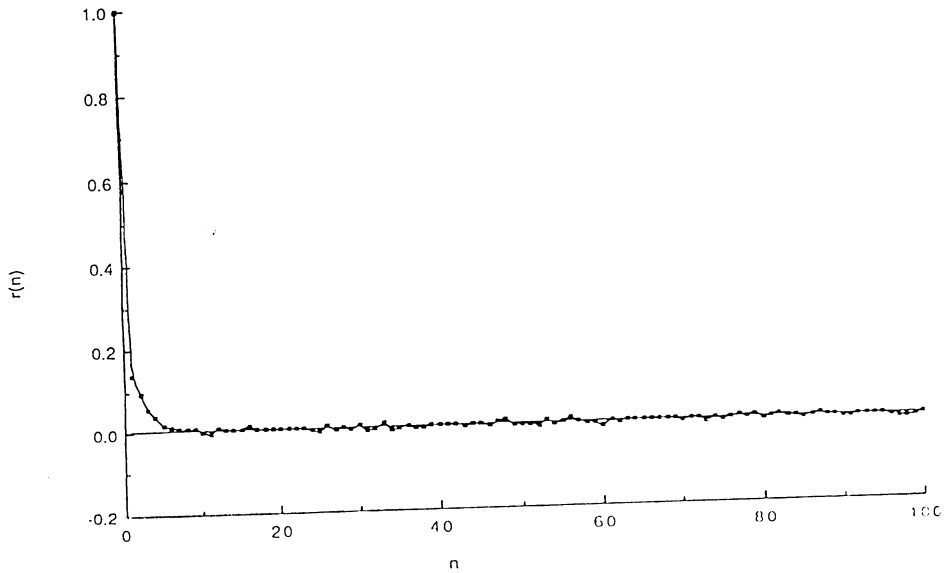

Fig. 13. The autocorrelation sequence for the Lorenz attractor, N = 76,000.

the correlation time for the autocorrelation, $M > 2$ for the chaotic bubble, $M > 5$ for the Lorenz attractor.

We can replace (8) with

$$\lambda(t_{N+1} - t_1) = \sum_{k=1}^{N} \log_2 \frac{\bar{d}(k+1)}{\bar{d}_0(k)} \tag{9}$$

where $\bar{d}_0(k)$ is the average "distance" between two statistically independent strings at the kth observation. If the two symbols at the $k+1$st observation have the same sign we say that the "distance" is unchanged, on the average

$$\bar{d}(k+1) = \bar{d}_0(k). \tag{10}$$

If the two symbols have different signs after one observation, then

$$\bar{d}(k+1) = c_1 \bar{d}_0(k) \tag{11}$$

where c_1 is the constant average change of distance. It follows from (10) and (11) that

$$\log_2 \frac{\bar{d}(k+1)}{\bar{d}_0(k)} = \begin{cases} 0 & \text{same sign} \\ \alpha & \text{sign change after iteration} \end{cases} \tag{12}$$

where $\alpha = \log_2 c_1$.

We now define the set S_1 of ergodic initial distance between strings of symbols

$$S_1 = \{k : u(k)u(k+M) = 1\}. \tag{13}$$

The complementary set is

$$S_2 = \{k : u(k)u(k+M) = -1\}. \tag{14}$$

Hence, we may write

$$\log_2 \frac{\bar{d}(k+1)}{\bar{d}_0(k)} = \frac{\alpha}{2}\{1 - u(k+1)u(k+1+M)\}$$

for all symbol sequences which have the same sign at the time k for all $k \in S_1$. Hence,

$$\sum_{k=1}^{N} \log_2 \frac{\bar{d}(k+1)}{\bar{d}_0(k)} = \frac{\alpha}{2} \sum_{k \in S_1} \{1 - u(k+1)u(k+1+M)\}. \tag{15}$$

The total number of k is N. Let N_1, N_2 be the number of k's in the sets S_1, S_2, and $N_1 + N_2 = N$. We have also that

$$N r(M) = \sum_{k=1}^{N} u(k)u(k+M) = \sum_{k \in S_1} u(k)u(k+M)$$
$$+ \sum_{k \in S_2} u(k)u(k+M) = N_1 - N_2 = 0. \tag{16}$$

Since $r(M) = 0$ when M is larger than the correlation "time." Hence $N_1 = N_2 = \frac{N}{2}$.

We next define the macroscopic Lyapunov exponent as the average value

$$\lambda_m = \frac{1}{N_1} \sum_{k \in S_1} \log_2 \frac{\bar{d}(k+1)}{\bar{d}_0(k)}$$
$$= \frac{\alpha}{N} \sum_{k \in S_1} \{1 - u(k+1)u(k+1+M)\}. \tag{17}$$

This is related to the average Lyapunov exponents by

$$\frac{\lambda(t_{N+1} - t_1)}{N} = \lambda_M. \tag{18}$$

Singh and Joseph (1989) showed that

$$\lambda_m = \frac{\alpha}{2}[1 - r^2(1)]. \tag{19}$$

<u>Lyapunov exponents and white noise</u>

Singh and Joseph (1989) calculated the macroscopic Lyapunov exponent for the Lorenz system described in the section, "Binary sequences." They calculate α as follows. The average distance between starting trajectories on the line AB (= CD) of Figure 11 is

$$\frac{|AB|}{3} = \bar{d}_0(k).$$

The switching distance is $|AD| - |AB| = \bar{d}(k+1)$. Hence

$$\frac{\bar{d}(k+1)}{\bar{d}_0(k)} = 3\left[\frac{|AD|}{|AB|} - 1\right].$$

They found that $|AD| = 4.31|AB|$. Then from (12) we calculate $\alpha = 3.3$. The relation (18) between the average Lyapunov exponent λ and the macroscopic exponent λ_M may be simplified by putting $t_{N+1} - t_1 = N\Delta T$ where ΔT is the average period. Then

$$\bar{\lambda} = \frac{\lambda_m}{\Delta T} = \frac{\alpha}{2\Delta T}\left(1 - r(1)^2\right)$$

where $\Delta T = 0.7519$ sec. We get

$$\lambda_m = 1.618 \text{bits/period} .$$

The largest Lyapunov exponents computed directly for the Lorenz attractor is

$$\lambda = 1.30 \text{ bits/period} .$$

Feeny and Moon (1989) have studied a chaotic dry friction oscillator using the method of binary sequences of Singh and Joseph (1989). They did an experiment with sliding friction in which an imposed change of the normal force caused the slider to stick. They also modeled their experiment with a second order forced ODE involving friction coefficient and normal load functions. They did Poincaré sections for the experiments with 2,048 symbols and for the differential equation with 10,000 symbols. The symbols form a string of binary numbers ± 1 corresponding to whether the motion is sticking or slipping at each pass through the Poincaré section. They measure distance on the Poincaré plot:

$$\bar{d}_0(k) = \frac{1}{3}, \; \bar{d}(k+1) = 1 .$$

Hence, using (19), they get $\alpha = \log_2 3 = 1.585$.

Feeny and Moon studied the tent map and logistic map using the formula (19) with $\alpha = 1.585$. They calculated r(1) for $N = 10^5$ and $N = 2048$. The theoretical value of the largest Lyapunov exponent is $\lambda = 1$ for both the tent map and the logistic map. They compute

$$\lambda_m = \left.\begin{matrix} 0.787515 \;\; (10^5 \text{ symbols}) \\ 0.787705 \;\; (2048 \text{ symbols}) \end{matrix}\right\} \text{tent map}$$

$$\lambda_m = \left.\begin{matrix} 0.791578 \;\; (10^5 \text{ symbols}) \\ 0.791116 \;\; (2048 \text{ symbols}) \end{matrix}\right\} \text{logistic map}$$

A binary autocorrelation was obtained for their experiments and numerically from the differential equation for a symbol string with $N = 2048$. In both cases the autocorrelation r(1) is very small, less than ± 0.05. They calculate

$$\lambda_m = \begin{cases} 0.79055 \;\; \text{experiment} \\ 0.79219 \;\; \text{numerical integration} \end{cases}$$

The calculation of the exponent for the Poincaré map from the equations of motion gives

$$\lambda = 0.77 .$$

We draw the reader's attention to the fact that for all the calculations done by Feeny and Moon, they get

$$\lambda_m = \frac{\alpha}{2}\left[1 - r(1)^2\right] = 0.7925\left[1 - r(1)^2\right].$$

This shows that $r(1)^2$ is very small in the examples of the tent map, logistic map and experiments.

Short range predictability requires that r(1), r(2), ..., r(M) $\neq 0$ for small M, $r(n) \to 0$ for large n. For white noise, we have $r(1) = 0$. The autocorrelation is good for distinguishing short range predictability and white noise. The macroscopic Lyapunov exponent is not useful for making this important distinction. In fact, the macroscopic Lyapunov exponent depends on distance through α, but λ_m / α is universal, does not depend on distance and may be a more intrinsic measure of chaos. Certainly r(1) has a lot less information than the graph of r(n).

REFERENCES

Feeny, B.F. and Moon, F.C., 1990, Autocorrelation on symbol dynamics for a chaotic dry friction oscillation, *Phys. Letters A* (to appear).

Fortes, A., Joseph, D.D., and Lundgren, T.S., 1987, Nonlinear mechanics of fluidization of beds of spherical particles, *J. Fluid Mech.,* 177:467-483.

Guillopé, C., Joseph, D.D., Nguyen, K., and Rosso, F., 1987, Nonlinear stability of rotating flow of two fluids, *J. Theoretical & Applied Mech.,* 6:619-645.

Joseph, D.D., Nguyen, K., and Beavers, G.S., 1984, Nonuniqueness and stability of the configuration of flow of immiscible fluids with different viscosities, *J. Fluid Mech.,* 141:319-345.

Joseph, D.D., Preziosi, L., 1987, Stability of rigid motions and coating films in bicomponent flows of immiscible liquids, *J. Fluid Mech.,* 185:323-351.

Renardy, Y. and Joseph D.D., 1985, Couette flow of two fluids between concentric cylinders. *J. Fluid Mech.,* 150:381-394.

Singh, P. and Joseph, D.D., 1989, Autoregressive methods for chaos on binary sequences for the Lorenz attractor, *Phys. Letters A*, 135:247-253.

Recent IMA Preprints

#	Author/s	Title
547	**M. Slemrod**,	Dynamics of Measured Valued Solutions to a Backward-Forward Heat Equation
548	**Avner Friedman and Jürgen Sprekels**,	Steady States of Austenitic–Martensitic–Domains in the Ginzburg–Landau Theory of Shape Memory Alloys
549	**Avner Friedman and Bei Hu**,	Degenerate Hamilton–Jacobi–Bellman Equations in a Bounded Domain
550	**E.G. Kalnins, Willard Miller, Jr., and M.V. Tratnik**,	Families of Orthogonal and Biorthogonal Polynomials on the N-Sphere
551	**Heinrich Freistühler**,	On Compact Linear Degeneracy
552	**Matthew Witten**,	Quantifying the Concepts of Rate and Acceleration/Deceleration of Aging
553	**J.P. Albert and J.L. Bona**,	Total Positivity and the Stability of Internal Waves in Stratified Fluids of Finite Depth
554	**Brian Coomes and Victor Zurkowski**,	Linearization of Polynomial Flows and Spectra of Derivations
555	**Yuriko Renardy**,	A Couette-Poiseuille Flow of Two Fluids in a Channel
556	**Michael Renardy**,	Short wave instabilities resulting from memory slip
557	**Daniel D. Joseph and Michael Renardy**,	Stokes' first problem for linear viscoelastic fluids with finite memory
558	**Xiaxi Ding**,	Superlinear Conservation Law with Viscosity
559	**J.L. Ericksen**,	Liquid Crystals with Variable Degree of Orientation
560	**F. Robert Ore, Jr. and Xinfu Chen**,	Electro-Optic Modulation in an Arbitrary Cross-Section Waveguide
561	**M.V. Tratnik**,	Multivariable biorthogonal continuous-discrete Wilson and Racah polynomials
562	**Yisong Yang**,	Existence of Solutions for a Generalized Yang-Mills Theory
563	**Peter Gritzmann, Laurent Habsieger and Victor Klee**,	Good and Bad Radii of Convex Polygons
564	**Martin Golubitsky, Martin Krupa and Chjan. C. Lim**,	Time-Reversibility and Particle Sedimentation
565	**G. Yin**,	Recent Progress in Parallel Stochastic Approximations
566	**G. Yin**,	On H-Valued SA: Finite Dimensional Approximations
567	**Chien-Cheng Chang**,	Accurate Evaluation of the Effect of Diffusion and Conductivity in Certain Equations
568	**Chien-Cheng Chang and Ruey-Ling Chern**,	The Effect of Viscous Diffusion in Discrete Vortex Dynamics for Slightly Viscous Flows
569	**Li Ta-Tsien (Li Da-qian) and Zhao Yan-Chun**,	Global Existence of Classical Solutions to the Typical Free Boundary Problem for General Quasilinear Hyperbolic Systems and its Applications
570	**Thierry Cazenave and Fred B. Weissler**,	The Structure of Solutions to the Pseudo-Conformally Invariant Nonlinear Schrödinger Equation
571	**Marshall Slemrod and Athanasios E. Tzavaras**,	A Limiting Viscosity Approach for the Riemann Problem in Isentropic Gas Dynamics
572	**Richard D. James and Scott J. Spector**,	The Formation of Filamentary Voids in Solids
573	**P.J. Vassiliou**,	On the Geometry of Semi-Linear Hyperbolic Partial Differential Equations in the Plane Integrable by the Method of Darboux
574	**Jerome V. Moloney and Alan C. Newell**,	Nonlinear Optics
575	**Keti Tenenblat**,	A Note on Solutions for the Intrinsic Generalized Wave and Sine-Gordon Equations
576	**P. Szmolyan**,	Heteroclinic Orbits in Singularly Perturbed Differential Equations
577	**Wenxiong Liu**,	A Parabolic System Arising In Film Development
578	**Daniel B. Dix**,	Temporal Asymptotic Behavior of Solutions of the Benjamin-Ono-Burgers Equation
579	**Michael Renardy and Yuriko Renardy**,	On the nature of boundary conditions for flows with moving free surfaces
580	**Werner A. Stahel**,	Robust Statistics: From an Intellectual Game to a Consumer Product
581	**Avner Friedman and Fernando Reitich**,	The Stefan Problem with Small Surface Tension
582	**E.G. Kalnins and W. Miller, Jr.**,	Separation of Variables Methods for Systems of Differential Equations in Mathematical Physics
583	**Mitchell Luskin and George R. Sell**,	The Construction of Inertial Manifolds for Reaction-Diffusion Equations by Elliptic Regularization
584	**Konstantin Mischaikow**,	Dynamic Phase Transitions: A Connection Matrix Approach
585	**Philippe Le Floch and Li Tatsien**,	A Global Asymptotic Expansion for the Solution to the Generalized Riemann Problem
586	**Matthew Witten, Ph.D.**,	Computational Biology: An Overview
587	**Matthew Witten, Ph.D.**,	Peering Inside Living Systems: Physiology in a Supercomputer

Recent IMA Preprints (Continued)

#	Author/s	Title
588	**Michael Renardy**,	An existence theorem for model equations resulting from kinetic theories of polymer solutions
589	**Daniel D. Joseph and Luigi Preziosi**,	Reviews of Modern Physics: Addendum to the Paper "Heat Waves"
590	**Luigi Preziosi**,	An Invariance Property for the Propagation of Heat and Shear Waves
591	**Gregory M. Constantine and John Bryant**,	Sequencing of Experiments for Linear and Quadratic Time Effects
592	**Prabir Daripa**,	On the Computation of the Beltrami Equation in the Complex Plane
593	**Philippe Le Floch**,	Shock Waves for Nonlinear Hyperbolic Systems in Nonconservative Form
594	**A.L. Gorin, D.B. Roe and A.G. Greenberg**,	On the Complexity of Pattern Recognition Algorithms On a Tree-Structured Parallel Computer
595	**Mark J. Friedman and Eusebius J. Doedel**,	Numerical computation and continuation of invariant manifolds connecting fixed points
596	**Scott J. Spector**,	Linear Deformations as Global Minimizers in Nonlinear Elasticity
597	**Denis Serre**,	Richness and the classification of quasilinear hyperbolic systems
598	**L. Preziosi and F. Rosso**,	On the stability of the shearing flow between pipes
599	**Avner Friedman and Wenxiong Liu**,	A system of partial differential equations arising in electrophotography
600	**Jonathan Bell, Avner Friedman, and Andrew A. Lacey**,	On solutions to a quasilinear diffusion problem from the study of soft tissue
601	**David G. Schaeffer and Michael Shearer**,	Loss of hyperbolicity in yield vertex plasticity models under nonproportional loading
602	**Herbert C. Kranzer and Barbara Lee Keyfitz**,	A strictly hyperbolic system of conservation laws admitting singular shocks
603	**S. Laederich and M. Levi**,	Qualitative dynamics of planar chains
604	**Milan Miklavčič**,	A sharp condition for existence of an inertial manifold
605	**Charles Collins, David Kinderlehrer, and Mitchell Luskin**,	Numerical approximation of the solution of a variational problem with a double well potential
606	**Todd Arbogast**,	Two-phase incompressible flow in a porous medium with various nonhomogeneous boundary conditions
607	**Peter Poláčik**,	Complicated dynamics in scalar semilinear parabolic equations in higher space dimension
608	**Bei Hu**,	Diffusion of penetrant in a polymer: a free boundary problem
609	**Mohamed Sami ElBialy**,	On the smoothness of the linearization of vector fields near resonant hyperbolic rest points
610	**Max Jodeit, Jr. and Peter J. Olver**,	On the equation grad $f = M$ grad g
611	**Shui-Nee Chow, Kening Lu, and Yun-Qiu Shen**,	Normal form and linearization for quasiperiodic systems
612	**Prabir Daripa**,	Theory of one dimensional adaptive grid generation
613	**Michael C. Mackey and John G. Milton**,	Feedback, delays and the origin of blood cell dynamics
614	**D.G. Aronson and S. Kamin**,	Disappearance of phase in the Stefan problem: one space dimension
615	**Martin Krupa**,	Bifurcations of relative equilibria
616	**D.D. Joseph, P. Singh, and K. Chen**,	Couette flows, rollers, emulsions, tall Taylor cells, phase separation and inversion, and a chaotic bubble in Taylor-Couette flow of two immiscible liquids
617	**Artemio González-López, Niky Kamran, and Peter J. Olver**,	Lie algebras of differential operators in two complex variables
618	**L.E. Fraenkel**,	On a linear, partly hyperbolic model of viscoelastic flow past a plate
619	**Stephen Schecter and Michael Shearer**,	Undercompressive shocks for nonstrictly hyperbolic conservation laws
620	**Xinfu Chen**,	Axially symmetric jets of compressible fluid
621	**J. David Logan**,	Wave propagation in a qualitative model of combustion under equilibrium conditions
622	**M.L. Zeeman**,	Hopf bifurcations in competitive three-dimensional Lotka-Volterra Systems
623	**Allan P. Fordy**,	Isospectral flows: their Hamiltonian structures, Miura maps and master symmetries
624	**Daniel D. Joseph, John Nelson, Michael Renardy, and Yuriko Renardy**,	Two-Dimensional cusped interfaces